Research paper

Capacitive water release and internal leaf water relocation delay drought-induced cavitation in African *Maesopsis eminii*

Jackie Epila[1,2,5,†], Niels J.F. De Baerdemaeker[1,†], Lidewei L. Vergeynst[1], Wouter H. Maes[1,3], Hans Beeckman[4] and Kathy Steppe[1]

[1]Laboratory of Plant Ecology, Department of Applied Ecology and Environmental Biology, Faculty of Bioscience Engineering, Ghent University, Coupure links 653, B-9000 Ghent, Belgium; [2]CAVElab Computational & Applied Vegetation Ecology, Department of Applied Ecology and Environmental Biology, Ghent University, Coupure links 653, B-9000 Ghent, Belgium; [3]Remote Sensing, University of Technology Sydney (UTS), 745 Harris Str., Broadway 2007, NSW, Australia; [4]Laboratory for Wood Biology and Xylarium (Royal Museum for Central Africa), Leuvensesteenweg 13, B-3080 Tervuren, Belgium; [5]Corresponding author (Jackie.Epila@UGent.be)

The impact of drought on the hydraulic functioning of important African tree species, like *Maesopsis eminii* Engl., is poorly understood. To map the hydraulic response to drought-induced cavitation, sole reliance on the water potential at which 50% loss of xylem hydraulic conductivity (ψ_{50}) occurs might be limiting and at times misleading as the value alone does not give a comprehensive overview of strategies evoked by *M. eminii* to cope with drought. This article therefore uses a methodological framework to study the different aspects of drought-induced cavitation and water relations in *M. eminii*. Hydraulic functioning of whole-branch segments was investigated during bench-top dehydration. Cumulative acoustic emissions and continuous weight measurements were used to quantify *M. eminii*'s vulnerability to drought-induced cavitation and hydraulic capacitance. Wood structural traits, including wood density, vessel area, diameter and wall thickness, vessel grouping index, solitary vessel index and vessel wall reinforcement, were used to underpin observed physiological responses. On average, *M. eminii*'s ψ_{50} ($\pm$SE) was -1.9 ± 0.1 MPa, portraying its xylem as drought vulnerable, just as one would expect for a common tropical pioneer. However, *M. eminii* additionally employed an interesting desiccation delay strategy, fuelled by internal relocation of leaf water, hydraulic capacitance and the presence of parenchyma around the xylem vessels. Our findings suggest that exclusive dependence on ψ_{50} would have misdirected our assessments of *M. eminii*'s drought stress vulnerability. Hydraulic capacitance linked to anatomy and leaf-water relocation behaviour was equally important to better understand *M. eminii*'s drought survival strategies. Because our study was conducted on branches of 3-year-old greenhouse-grown *M. eminii* seedlings, the findings cannot be simply extrapolated to adult *M. eminii* trees or their mature wood, because structural and physiological plant properties change with age. The techniques and methodological framework used in this study are, however, transferable to other species regardless of age.

Keywords: acoustic emissions, anatomy, desiccation time, drought stress, embolism, hydraulic capacitance, tropical seedlings, vulnerability curve.

Introduction

Maesopsis eminii Engl. is a forest tree species of economic importance to tropical Africa due to its versatile uses (Eggeling 1947, Hall 1995). Aside from this, *M. eminii* possesses unique characteristic attributes. These include (i) its remarkable ecological feat

that allows it to straddle the equator to 10.97 N and 10.98 S in regions with a mean rainfall range of 657–3217 mm year^{-1}; (ii) its ability to thrive in different African ecosystems, including rainforests, riverine forests (Schabel and Latiff 1997), mixed swamp forests (Eggeling 1947, Jenkin et al. 1977), shrub-dominated

[†]These authors contributed equally to this work.

transition zones that separate forests from grasslands (Hall 1995), between high forests and savannah (Orwa et al. 2009), lowland and submontane forests (Binggeli and Hamilton 1993), and countries outside Africa such as Australia, the Philippines, Bangladesh, Brazil, Costa Rica, Fiji, India, Malaysia, Samoa, Solomon Islands, Hawaii, Puerto Rico and Indonesia (Buchholz et al. 2010, Hall 2010, CABI 2016); (iii) its functional traits, which include pioneer characteristics, drought-deciduous leaves, ability to tolerate drought for up to 6 months, invasive nature, fast growth capability, high light demand (Eggeling 1947, Hall 1995) and low wood density (0.37–0.48 g cm^{-3}) (Chave et al. 2009); and (iv) its family being Rhamnaceae (Eggeling 1947, Hall 1995), which includes many extremely drought-tolerant species. These summed characteristics theoretically suggest that *M. eminii* most likely possesses physiological and structural properties that allow it to cope with drought-induced cavitation which, according to the hypothesis postulated by Zimmermann (1983), is induced by air-seeding through the pore of an inter-conduit membrane. This theory is widely accepted (Shen et al. 2002, De Roo et al. 2016), and was recently updated by Schenk et al. (2015), who emphasized the formation of nano-bubbles prior to cavitation to account for the stability of gas bubbles under negative pressure.

To fully understand drought responses in woody species, we have to consider that a trade-off exists between hydraulic efficiency and hydraulic safety (Sperry et al. 2008). Higher efficiency is associated with greater conduit dimensions, higher vessel connectivity and a higher degree of vessel grouping (Carlquist 1984, Loepfe et al. 2007). The more efficient the xylem network, the higher the hydraulic conductivity, photosynthetic capacity and plant growth (Loepfe et al. 2007). Additionally, high efficiency permits lower xylem construction and maintenance cost per unit transpiration (Gleason et al. 2016). Contrastingly, the more resistant the xylem network, the better the plant performance will be under higher xylem tension, allowing plants to operate in dry soils and enabling them to keep transpiring for longer periods during the day or year (Gleason et al. 2016). Hydraulic safety is typically associated with a smaller size of the pit aperture (Bouche et al. 2014). The reverse is true for hydraulic efficiency: according to the rare pit hypothesis, conduits with larger pit size are more susceptible to air entry as they are likely to possess 'rare' pores of air-seeding size (Christman et al. 2009). In addition to pit size, the hydraulic capacitance (*C*) might play an important role in guaranteeing hydraulic safety even in dry habitats (Gleason et al. 2016). The hydraulic capacitance is theoretically defined as the ratio of change in tissue volumetric water content to change in xylem water potential (Vergeynst et al. 2015a), and can be measured as the amount of water released from the tissue per unit decrease in water potential (Edwards and Jarvis 1982, Steppe and Lemeur 2007). Indeed, plants with a high *C* can temporarily ward off cavitation by releasing stored water into the

transpiration stream from different organs and tissue types (Sperry et al. 2008, Meinzer et al. 2009, Steppe et al. 2012, Vergeynst et al. 2015a).

To characterize the sensitivity of a plant species to drought stress, a vulnerability curve (VC) is usually developed (Pammenter and Van der Willigen 1998, Meinzer et al. 2009) from which the universal index, ψ_{50}, is determined. This value represents the tension at which 50% loss of xylem hydraulic conductivity occurs (Choat et al. 2012). The ψ_{50} values enlisted by Choat et al. (2012) capture multiple species from different continents, but African tree species' drought vulnerability was only reflected by Tunisian and South African tree species. The few available Africa-related studies mirror how uncertain we are of African tree species' responses to drought, especially now that the intensity and frequency of drought events are more pronounced because of climatic change (Asefi-Najafabady and Saatchi 2013).

Although ψ_{50} is often used as a single index of a plant's sensitivity to drought stress, a suite of physiological, allometric and anatomical traits that reduce the risk of potential xylem dysfunction (Barnard et al. 2011) can be equally important. Such traits can be either physio-morphological or structural. Physio-morphological traits include deep rooting, strict stomatal control and control of leaf area, e.g., through leaf shedding (Pineda-García et al. 2013). Examples of structural traits that determine functionality during low soil water conditions are low wood density (Borchert 1994) linked to high hydraulic capacitance and low xylem construction cost, narrow inter-conduit pit pores, low degree of vessel connectivity and high conduit wall reinforcement (Hacke and Sperry 2001, McCulloh et al. 2012, Scholz et al. 2013).

In this article, we use a generic methodological framework to study different aspects of drought-induced cavitation and water relations in the species *M. eminii*. The techniques include: (i) VCs performed with acoustic emission (AE) sensors using the cumulative number of AE signals to quantify the ψ_{50} value (Rosner et al. 2009, Vergeynst et al. 2015a); (ii) leaf and stem water potential (ψ_{leaf} and ψ_{xylem}) measurements performed with the pressure bomb technique to discern water tension within the plant (Begg and Turner 1970); (iii) relative radial xylem diameter shrinkage as an additional indicator for water tension (Irvine and Grace 1997); (iv) branch gravimetrical water loss to give insights into the consecutive phases of dehydration and to quantify hydraulic capacitance (Vergeynst et al. 2015a); (v) wood anatomy to understand the role of structural traits in cavitation impairment; and (vi) wood density as an indirect method to quantify cavitation vulnerability (Borchert 1994, Rosner et al. 2013).

The methodological framework was applied to examine the vulnerability to drought of whole-branch segments of 3-year-old greenhouse-grown seedlings of the African tree species *M. eminii*. The main objective of our study was to use the sets of techniques to assess the hydraulic functioning of *M. eminii* seedlings and to determine which physiological and structural

characteristics contribute to the species' drought-coping ability. Because experience has demonstrated that it requires several weeks of drought stress to induce cavitation in intact trees (Cochard et al. 2013), bench-top dehydration of long leafy branch segments was applied to induce cavitation.

Materials and methods

Experimental set-up

Maesopsis eminii Engl. seeds from unselected parent plants were randomly collected from Uganda's Mabira forest reserve floor in October 2012 (0°23.357′N, 33°0.344′E). Mabira is a secondary forest whose vegetation types represent sub-climax forest communities predominantly occupied by tropical high forest communities of medium altitude moist semi-deciduous and moist evergreen forests (Baranga 2007). *Maesopsis eminii* is one of the most frequently harvested commercial timber trees in Mabira (Baranga 2007). The reserve receives an annual rainfall of 1200–1400 mm between March–May and September–November (Boffa et al. 2008). The sourced seeds were grown in the tropical greenhouse facility of Ghent University, Belgium (50°59.58′N, 3°47.04′E) in 35-l pots containing peat soils. The seedlings were well-watered and fertilized throughout the entire period and were harvested at the age of 3 years. Chemistry of the irrigation water consisted of a mix of rainwater and soluble fertilizer with an NPKMg ratio of 19:8:16:4, boron (0.02%), copper (0.03%), iron (0.038%), manganese (0.05%), molybdenum (0.02%) and zinc (0.01%), resulting in a solution of pH 5.7. Climatic conditions were automatically controlled by a HortiMaX MT/MTV sensor Unit (Hortimax, Honderdland 131, 2676 LT Maasdijk, The Netherlands). Greenhouse air temperature (T) ranged between 18 and 36 °C, daily photosynthetic active radiation ranged between 0 and 2044 μmol m^{-2} s^{-1} and relative humidity between 24% and 96%. Each day, lights were turned on at 8 a.m. and off at 8 p.m. At the time of sampling, the seedlings had an average ($\pm$SD) height of 2.3 $\pm$ 0.4 m and an average ($\pm$SD) stem diameter of 28.3 $\pm$ 5.4 mm, measured approximately 2 m below the apex.

Sampling procedure

A total of five seedlings were used for the VC and hydraulic capacitance experiments. Experiments were performed using two alternating branches excised from each of these five *M. eminii* seedlings; 10 branches in total. Branch selection and preconditioning occurred a day prior to the start of the experiment, and was based on length (~70 cm), diameter (~7.0 $\pm$ 0.3 mm), alternating positioning on the stem and availability of a sufficient number of leaves (~100). Leaves of the five branches dedicated to drought vulnerability characterization (henceforth referred to as Set 1) were wrapped with aluminium foil to ensure equilibrium between leaf and stem water potential (Begg and Turner 1970) and branches were additionally covered with double-packed

black polythene bags. A similar procedure was followed for the second set of five branches used for hydraulic capacitance determination (henceforth referred to as Set 2), with exception of the individual leaf-foil wrapping. The five selected seedlings were watered to runoff to ensure complete hydration 15 h before branch excision. Aside from this pre-watering, overnight watering was repeated twice (8 p.m. and 11 p.m.) to guarantee complete plant hydration. Sampling was done predawn and branches of both sets were cut under water followed by two additional re-cuts of ~3 cm to avoid artifacts due to possible air entry (Cochard et al. 2013, Wheeler et al. 2013). The exposed parts of the branches were covered with wet cloth to keep the ends moist and to avoid dehydration during transport. The first measured water potential values for all branches were 0 MPa and no AE signals were registered during the first 30 min of dehydration, so we conclude that this wet cloth technique successfully avoided the occurrence of native emboli.

Measurements during dehydration

Excised branches were transported to the Laboratory of Plant Ecology, Ghent University (51°3.204′N, 3°42.511°E). The experimental room was darkened and equipped with an artificial green light to limit photosynthesis and transpiration when the black polythene bags were removed. After two separate sections of bark (1.5 × 0.5 cm^2) were removed with a scalpel to expose branch xylem, the five branches of Set 1 were equipped with a broadband point-contact AE sensor (KRNBB-PC, KRN Services, Richland, WA, USA) and a dendrometer (DD-S, Ecomatik, Dachau, Germany). The branches were also fixed in a custom-built holder to ensure a stable mount of both sensors, and an unbiased link between AE and diameter shrinkage.

The AE sensor was pressed to the exposed xylem via a compression spring (D22050, Tevema, Amsterdam, The Netherlands) in a small PVC tube. To ensure good acoustic contact, a droplet of vacuum grease was added between sensor tip and xylem, after which installation was validated via the pencil lead break test according to Vergeynst et al. (2015b). Petroleum jelly was also applied between dendrometer sensor tip and xylem to prevent evaporation from the exposed wound.

The five branches of Set 2 were stripped of all their leaves and petal wounds were covered with petroleum jelly to prevent loss of sap through the wound (Vergeynst et al. 2015a). These branches were placed on continuous weight balances (4× DK 6200 with 0.01 g accuracy and 2× PS 4500/C/1 with 0.1 g accuracy, Henk Maas, Veen, The Netherlands). Because the leaves of the Set 1 branches were completely covered with aluminium foil and those of Set 2 completely removed, it could be assumed that both sets of branches dehydrated in a similar way (Vergeynst et al. 2015a). Once both sets of branches were installed, wet cloths were removed and normal lights turned on.

Dendrometer and balance read-outs were registered every minute via custom-built acquisition boards. AE signals were

amplified by 35.6 dB (AMP-1BB-J, KRN Services, Richland, WA, USA), after which waveforms of 7168 sample length were acquired at 10 MHz sample rate. Signals were collected via 2-channel PCI boards and uploaded to the software program AEwin (PCI-2, AEwin E4.70, Mistras Group BV, Schiedam, The Netherlands). A 20–1000 kHz electronic band pass filter was applied, and only waveforms above the noise level of 28 dB$_{AE}$ were retained as described in Vergeynst et al. (2016).

Xylem water potential (ψ_{xylem}, MPa) was measured on wrapped excised leaves using the pressure chamber (PMS Instrument Company, Corvalis, OR, USA). When the frequency of new AE signals became higher, live-monitored with the AEwin software program, the time between consecutive pressure bomb readings was shortened. At the start of dehydration, measurements were frequent with a mean time interval of ~5 min. This interval increased for the subsequent measurement days to between 0.5 and 2 h, ending with a maximum of three readings from Day 3 onwards. For generating the stress–strain relation, all measured xylem water potential values were used.

Processing acoustic emission data

Following Vergeynst et al. (2015a) we translated the measured AE into meaningful percentage loss of hydraulic conductivity (PLC) by first cumulating the AE signals over the entire dehydration period. From the cumulative AE, the first derivative was calculated to produce the AE activity curve, after which second and third derivatives were calculated. The definition of Vergeynst et al. (2016) was used to determine the endpoint of the VC (ψ_{100}). Acoustic emission activity was calculated numerically over a time interval of 5 min, while second and third derivatives were quantified over 24 h due to the slow dehydration process. Translation to PLC (%) was obtained by re-scaling the cumulated AE signals from zero to ψ_{100}. Values corresponding with the onset of cavitation (ψ_{xylem} at 12%; ψ_{12}), 50% loss of conductivity (ψ_{xylem} at 50%; ψ_{50}) and at full embolism (ψ_{xylem} at 88%; ψ_{88}) were calculated as well.

Volumetric water content

Prior to the start of dehydration, a wood sample of ~5 cm in length was taken from each of the cut ends of the branches of Set 2. At the end of the bench-top dehydration, similar sampling was performed (Vergeynst et al. 2015a). The samples were weighed (Sartorius precision balance with 0.001 g accuracy, Sartorius Weighing Technology GmBH, Goettingen, Germany) and both diameter and length were determined via an automated caliper. These were then placed in paper bags and oven-dried at 80 °C for 2 weeks, after which the weight, length and diameter of the samples were re-determined. Sample volume was estimated assuming a cylindrical form after which initial and final water mass fraction and initial basic wood density (ρ_b, kg m^{-3}) (oven dry mass/green volume) were calculated following Vergeynst et al. (2015a). Volumetric water content (VWC, kg m^{-3}) was calculated by multiplying mass fraction with ρ_b, whilst the actual change in VWC was obtained by re-scaling the continuous weight data to the range of water contents between initial and final water content of the samples (Vergeynst et al. 2015a).

Stress–strain relation, modulus of elasticity and hydraulic capacitance

Relative radial xylem shrinkage ($\Delta d/d_i$) was determined using the initial diameter (d_i) prior to dehydration and the continuous diameter change (Δd; difference between the diameter after each 5 min consecutive time step (d_t) and the initial diameter (d_i)) monitored with the dendrometers (Irvine and Grace 1997:

$$\frac{\Delta d}{d_i} = \left(\frac{d_t - d_i}{d_i} \right) \tag{1}$$

Point measurements of ψ_{xylem} of the five branches (Set 1) were plotted versus their corresponding relative radial xylem shrinkage to produce a pooled stress–strain curve, from which the apparent modulus of elasticity in the radial direction (E_r', MPa) was obtained as the slope of the linear regression between pooled ψ_{xylem} and $\Delta d/d_i$ (Irvine and Grace 1997). This stress–strain relation was used to obtain continuous xylem water potential data that was used to produce the x-axis of the vulnerability and VWC curve (Vergeynst et al. 2015a). Plotting VWC against xylem water potential showed two regions of interest, separated by two distinct breakpoints. The first and second breakpoint indicate the start and end of Phase I, or the elastic shrinkage phase, and were calculated via the segmented R package (Muggeo 2008). The third breakpoint corresponds with ψ_{100} of the PLC curve, and the region between second and third breakpoint is known as the cavitation or inelastic shrinkage phase, or Phase II (Figures 1 and 3; Vergeynst et al. 2015a). Following the procedure of Vergeynst et al. (2015a), hydraulic capacitance for both phases was determined as follows:

$$C = \frac{dVWC}{d\psi_{xylem}} = \frac{dVWC}{d(\Delta d/d_i)} \left(\frac{d\psi_{xylem}}{d(\Delta d/d_i)} \right)^{-1} = \frac{dVWC}{d(\Delta d/d_i)}(E_r')^{-1} \tag{2}$$

In addition, we calculated overall hydraulic capacitance as the slope of the linear regression fitted through the entire data set.

Microscopic analysis

In order to visualize the origin of *M. eminii*'s hydraulic capacitance and to decipher wood anatomical traits, the anatomy of six additional branches with similar dimensions to the branches used for vulnerability assessment, were analysed. Branch samples, which were excised at a 40 cm distance from branch tip to mimic sensor positioning during the bench-top dehydration test,
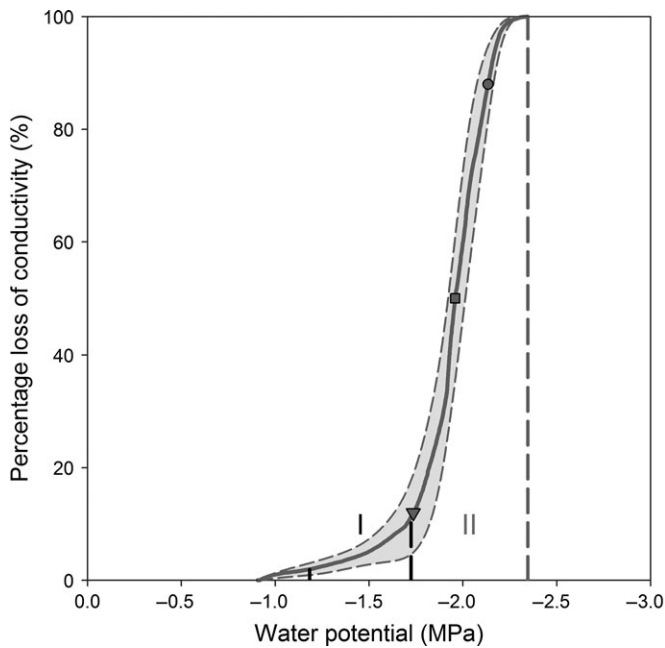
Figure 1. Illustration of *M. eminii*'s average VC with standard error margins obtained by plotting converted cumulative AE values as PLC against xylem water potential. Phases I and II are delimited by vertical lines, and the vulnerability thresholds ψ_{12} (triangle), ψ_{50} (square), ψ_{88} (circle) and ψ_{100} (dashed line) are indicated as well.

consecutively dehydrated for 3 min each, following the alcohol-concentration gradient of 50%, 75%, 96% and finally 100% ethanol. Once the dehydration process was done, the thin sections were transferred onto new cut-colour-frosted microscope slides (W × D × H; 76 × 26 × 1 mm³; VWR International Ltd, Hunter Blvd, Lutterworth LE17 4XN, UK), excess ethanol was drained by tilting the slides after which a microscopy mounting agent Euparal was added and the entire set-up covered using microscope cover glasses to make permanent slides. This completed set-up was then labelled, weights were placed on them, and they were allowed to dry for 3 days and thereafter analysed microscopically.

Complete transverse sections were transformed into images using an automated OLYMPUS BX60 microscope with a motorized positioning stage (Märzhäuser GmbH & Co. KG, In der Murch 15, 35579 Wetzlar, Germany; 100 × 100 mm² travel range; ball screw pitch of 1 mm) that allowed complete capture of the sections. These were visualized using the OLYMPUS Stream Motion 1.8 software, for which a 10× objective magnification was used. To allow for more detail, cross-sections were also divided into four quadrants and visualised by a 20× objective magnification. Images were then processed with ArcGIS 10.2.2 (ESRI, Redlands, CA, USA). Entire transverse sections were further analysed for vessel grouping index (V_G (–), the ratio of the total number of vessels to the total number of vessel groupings (sum of solitary vessels + vessel clusters + radial multiples)) and solitary vessel index (V_S (–), the ratio of total number of solitary vessels to the total number of vessel grouping including solitary and grouped vessels) (Scholz et al. 2013). The average vessel area (μm²) was determined, from which mean vessel diameter (μm) was obtained by assuming a circular vessel shape. In addition, xylem wood area was deduced from the micrograph to allow the calculation of ratios of total vessel area to xylem wood area. Thickness of the double wall between two vessels, t (μm) and span or vessel diameter b (μm) were measured manually using the ImageJ 1.47 v software. Vessel wall reinforcement $(t/b)^2$ (–) was then calculated and averaged over the four separate quadrants following Hacke and Sperry (2001).

Results

Branches of *M. eminii* had an average (±SD) basic wood density (ρ_b) of 302 ± 21 kg m⁻³ and an average (±SD) initial volumetric water content (VWC$_{init}$) of 750 ± 12 kg m⁻³. They were completely desiccated within 6 days.

The averaged VC curve of *M. eminii* with standard error bands was sigmoidal shaped (Figure 1) and resulted in an average (±SE) ψ_{12} of −1.7 ± 0.2 MPa (23.83 h, PLC: 12%), an average (±SE) ψ_{50} of −1.9 ± 0.1 MPa (48.75 h, PLC: 50%), an average (±SE) ψ_{88} of −2.1 ± 0.1 MPa (77.83 h, PLC: 88%) and an average (±SE) ψ_{100} of −2.3 ± 0.0 MPa (143.33 h, PLC: 100%). Even though this illustrates that *M. eminii* required a small decrease in xylem pressure to shift from onset of cavitation

were marked with white wash and preserved in separate labelled Ø54 mm containers containing a 20/40/40 ratio of ethanol (70% concentration), glycerin and distilled water. These were then taken to the wood lab of the Royal Museum for Central Africa, Tervuren-Belgium (50° 49.855′N, 4° 31.098′E) for microscopic analysis.

At the wood lab, samples were resized by cutting cross-sections of the branches with a miniature saw until a point near the 40 cm mark was reached. The six cut samples were then placed in ice trays and marked with paper tags. Hot polyethylene glycol (PEG) liquid was poured over the samples until the border of the tray was reached, and these were then placed in the oven at 80 °C for a period of 4 days and then removed for a day to allow PEG solidification in order to mummify the branch segments. These segments were then reshaped using a sharp knife after a spirit-level positioning was done for all the branch wood samples clamped inside the semi-automated microtome (Microm HM 440 E, GMI, Ramsey, MN, USA) sample holder. Microtome sectioning was done at a thickness of 12–16 μm. The obtained transverse sections were put on glass slides, covered with nylon and fastened into position using rubber bands. Residual PEG was washed off by dipping the sections in water after which they were placed in a zigzag manner in a custom-made holder. They were stained by placing them for 5 min in a container with a solution mix of 0.35 g Safranin in 35 ml 50% ethanol and 0.65 g Alcian blue in 65 ml DI water. The sample was then rinsed by dipping in distilled water and thereafter

(ψ_{12}) to fully embolized (ψ_{88}), the timespan for this transition expanded beyond 2 days.

As branch dehydration progressed, we noted for all five branches of Set 1 that some leaves on the same branch sampled at the same time had much lower water potentials values (more negative) while others had values that were less negative. This is reflected in the stress–strain curve by the large variability in ψ_{xylem} for similar values of $\Delta d/d_i$ during the entire dehydration process (Figure 2). The apparent modulus of elasticity in the radial direction (E'_r) was calculated as the slope of the linear regression fitted to the pooled stress–strain curve ($R^2 = 0.33$) and was 11 MPa. The P value was $3.0e^{-12}$ for the linear regression indicating that the used linear regression is justified for our stress–strain relation and apparent modulus of elasticity determination.

In Figure 3, the relationship between xylem water potential and VWC is shown. The elastic hydraulic capacitance ($C_{elastic}$, capacitance of Phase I) was on average ($\pm$SE) 319 ± 20 kg m^{-3} MPa^{-1} ($R^2 = 0.998$) and the inelastic capacitance ($C_{inelastic}$, capacitance of Phase II) was 655 ± 56 kg m^{-3} MPa^{-1} ($R^2 = 0.999$). The overall hydraulic capacitance was on average ($\pm$SE) 518 ± 38 kg m^{-3} MPa^{-1} ($R^2 = 0.967$). Volumetric water content decreased by 23% during the elastic phase and in total by 83% at the end of the inelastic phase (Figure 3).

Results from the branch wood anatomical analysis showed an average ($\pm$SD) vessel area of 1359 ± 767 μm^2, ranging between 300 and 5000 μm^2 (Figure 4). The average ($\pm$SD) vessel diameter was 40 ± 12 μm. Vessel walls were on average ($\pm$SD)

Figure 3. *Maesopsis eminii*'s average VWC with standard error margins plotted against xylem water potential during the bench dehydration experiment. Phases I and II are delimited by vertical lines and the slopes within these phases represent elastic ($C_{elastic}$) and inelastic ($C_{inelastic}$) hydraulic capacitance, respectively.
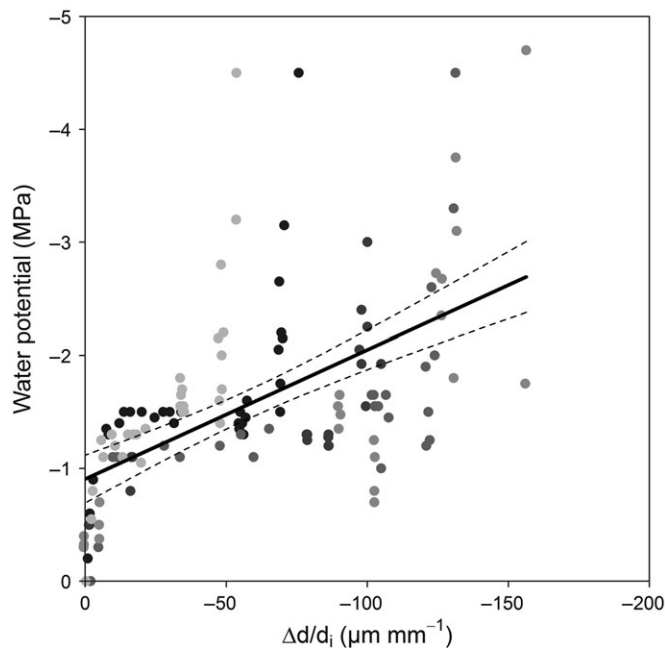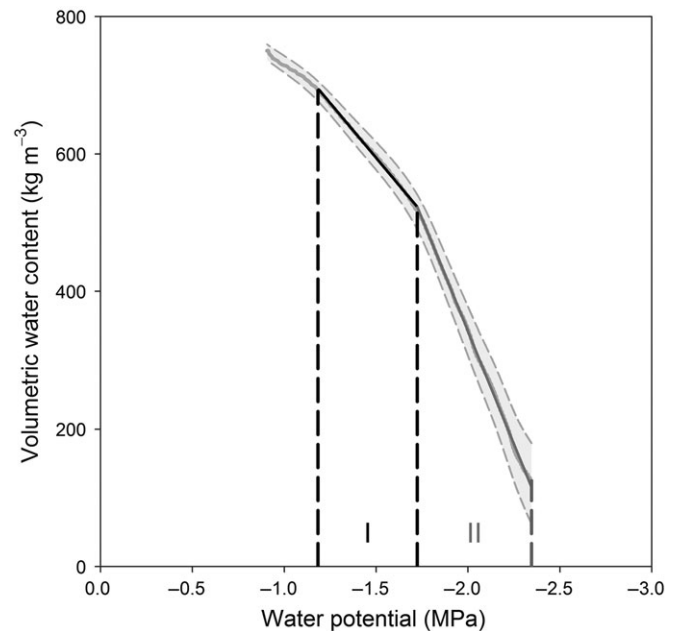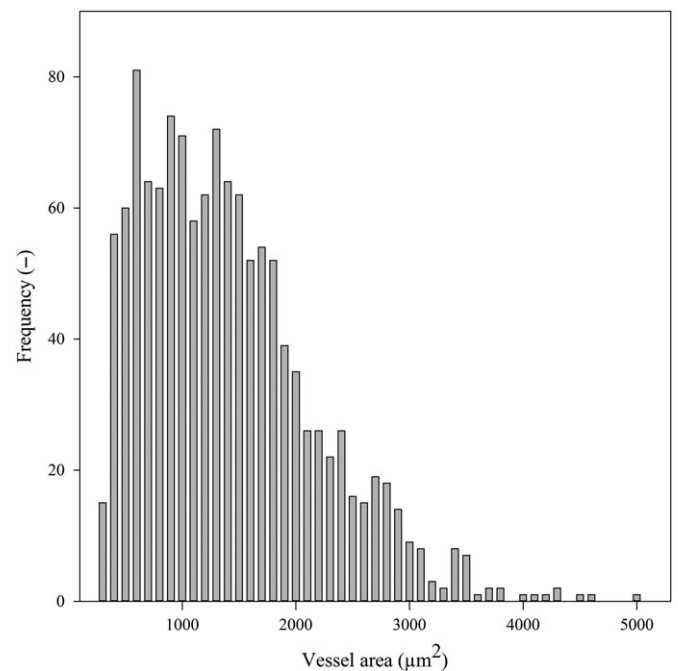

Figure 2. Stress–strain relationship of the examined *M. eminii* samples (circles) was obtained by plotting measured xylem water potential against corresponding relative radial xylem diameter shrinkage ($\Delta d/d_i$). The different shade colours indicate the five different branches. The linear regression was calculated for the pooled stress–strain relationship ($\psi = 0.011$ $\Delta d/d_i -$ 0.91; $R^2 = 0.33$). The dashed lines indicate a 95% confidence interval (P value: $3.0e^{-12}$). The variability between the samples and resulting low R^2 of the pooled relationship indicate how xylem water potential values varied due to internal leaf-water redistribution as branches dehydrated.

Figure 4. Branch wood hydraulic vessel area ($A = \pi r^2$) frequency distribution of *M. eminii* calculated from micrographs.

5.2 ± 1.1 µm thick. Only 8.3% of the entire xylem wood area was occupied by vessels, with the remaining area occupied by fibres, tracheids and parenchyma (Figure 5). Vessel wall reinforcement $(t/b)^2$ (−) was on average (±SD) 0.02 ± 0.01. Vessel grouping index V_G (−) and solitary vessel index V_S (−) were calculated from the micrograph (Figure 5) and were 1.52 and 0.61, respectively, indicating a high degree of solitary vessels.

Discussion

How vulnerable is M. eminii to drought-induced cavitation? Trade-off between safety and efficiency

The ψ_{50} value is widely used as a relevant and useful metric to quantify drought resistance across species (Anderegg 2015). We compared *M. eminii*'s average (±SE) ψ_{50} value of −1.9 ± 0.1 MPa, which was similar to Markesteijn et al. (2011) studied pioneer saplings (−1.8 ± 0.4 MPa), with Choat et al.'s values for other species to gauge *M. eminii*'s xylem vulnerability to drought-induced cavitation. Notwithstanding the fact that on average *M. eminii* achieved its ψ_{50} and ψ_{88} values respectively ~2 and ~3 days after the start of dehydration, our species was weighted vulnerable to drought-induced cavitation, because more than half of the species studied by Choat et al. (2012) had lower (more negative) values. Further confirmation of *M. eminii*'s vulnerability was ascertained after juxtaposing its ρ_b and $(t/b)^2$ against the curvilinear relationship ψ_{50} versus ρ_b and the linear relationship ψ_{50} versus $(t/b)^2$, which both portrayed *M. eminii* as sensitive to drought-induced cavitation (Hacke et al. 2000, 2001, Hacke and Sperry 2001, Pittermann et al. 2006, Hao et al. 2008, Rosner et al. 2013). Despite *M. eminii*'s V_G and V_S values indicating low vessel connectivity and vessel grouping
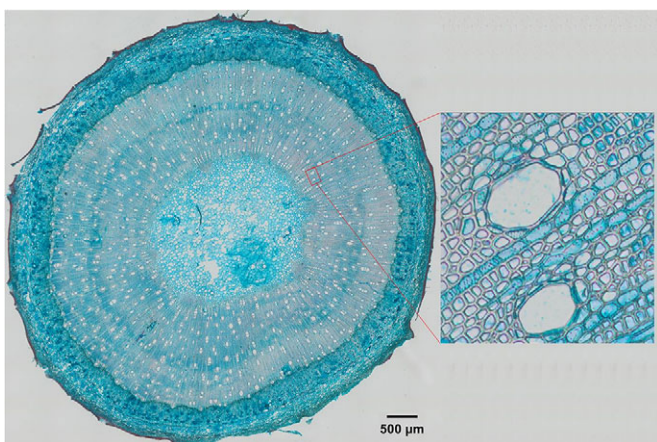

Figure 5. Optical micrograph of an entire stained thin section of a branch of the tropical diffuse-porous *M. eminii*, with the bark still intact, and stained with Safranin and Alcian blue. Regions coloured blue are associated with parenchyma and tension wood, the red portions are strongly lignified cell walls, vessels and fibres. Vessel grouping is also visible. The inset to the right depicts *M. eminii* hydraulic vessels being surrounded by parenchymatous cells.

that signify high hydraulic conduit safety and low hydraulic efficiency (Loepfe et al. 2007), *M. eminii*'s high average vessel diameter suggested a lower hydraulic safety. In their study, Christman et al. (2009) also associated wide vessels in *Acer* with a higher probability of leakier pits through which air-seeding can occur.

How vulnerable is vulnerable? Seeking desiccation-delay mechanisms

Reliance on these aforementioned parameters alone would lead to the wrong conclusion about how vulnerable *M. eminii*'s xylem is to drought-induced cavitation, because *M. eminii* seems to employ a desiccation-delay strategy (Figure 2). Ideally, as a branch dehydrates, one would expect the branch xylem water potential (ψ_{xylem}) value to linearly decline with time and diameter shrinkage (Figure 2). However, observation on dehydrating *M. eminii* branches defies the odds, as abnormally divergent ψ_{xylem} values were measured in all five dehydrating *M. eminii* branches. Per branch, some leaf values became more negative with drought as expected, while others in the same branch and at the same time tended to be less negative (Figure 2). These observations led us to speculate that as shrinkage and dehydration progressed, *M. eminii* progressively cut some leaves off from the water supply chain with the favoured ones remaining continuously supplied with 'redistributed' water, hence, their water potential tending to be less negative. This strategy may be a vital means of survival in the field where a few leaves are selected to support continued carbon fixation even during the dry season (Pearson et al. 2003), allowing light-demanding trees like *M. eminii* (Eggeling 1947) to quickly grow to higher light levels.

Maesopsis eminii's general stress–strain pattern (Figure 2) shows that, regardless of this 'redistribution' phenomenon, ψ_{xylem} values became more negative as shrinkage tended towards −50 µm mm^{-1}, which implies that xylem water became limiting. Between −50 and −125 µm mm^{-1}, however, some water potential values unexpectedly increased again (Figure 2), suggesting that a certain amount of water must be expelled from vessel-associated parenchyma localized around *M. eminii*'s hydraulic vessels that store water (Figure 5) to buffer the more negative water potentials. Once these internal water reserves ran out, water potentials became more negative again and this was irreversible (Figure 2). This internally stored water collectively contributes to the hydraulic capacitance (*C*) (Holbrook 1995). Therefore, *C*, defined as the amount of water released from the tissue per unit decrease in water potential (Edwards and Jarvis 1982, Steppe and Lemeur 2007), undoubtedly constitutes part of *M. eminii*'s 'redistribution' water. *Maesopsis eminii*'s *C* seems substantial as it delayed complete dehydration by 6 days and portrayed *M. eminii*'s safety margin (difference between onset of cavitation (ψ_{12}) and full embolism (ψ_{88}) (Domec and Gartner 2001, Meinzer et al. 2009) or 0.4 ± 0.1 MPa) as safe (Figure 1). We could substantiate this *C* using indicators such as *M. eminii*'s low basic wood

density values of $302 \pm 21 \, \text{kg m}^{-3}$ and high initial VWC (Figure 3), which both indicate a notable amount of stored water within *M. eminii*'s wood structure. In addition, VWC curves can be used to quantify hydraulic capacitance values (e.g., Vergeynst et al. 2015*a*). For *M. eminii*, hydraulic capacitance values were computed for two distinct phases (elastic and inelastic), and also the overall pooled one was calculated (Figure 3). Phase computations and related hydraulic capacitance data seldom exist in literature, and if they do exist (e.g., Meinzer et al. (2003, 2009) and McCulloh et al. (2012)), study conditions of measured branches vary from ours. Measurements are usually performed on samples sourced from much older and taller trees thriving within tropical forests and not in tropical greenhouses like ours, making direct comparison of our C_{elastic} ($319 \pm 20 \, \text{kg m}^{-3} \, \text{MPa}^{-1}$), $C_{\text{inelastic}}$ ($655 \pm 56 \, \text{kg m}^{-3} \, \text{MPa}^{-1}$) and pooled ($518 \pm 38 \, \text{kg m}^{-3} \, \text{MPa}^{-1}$) values with these field study values difficult. In spite of that, our study has shown that *M. eminii* relies on the participatory contribution of C during drought in prolonging the life span of some of its leaves (ψ_{xylem} values tending to less negative values during dehydration; Figure 2) with a significant C supply coming from the inelastic phase that is twice as high as the elastic amount (Figure 3). This supports the observed VC curve (Figure 1) and stress–strain (Figure 2) patterns, and is in line with the findings of Vergeynst et al. (2015*a*) who confirmed that water released by cavitation may significantly contribute to C under conditions of drought stress (Hölttä et al. 2009). *Maesopsis eminii* may thus be able to survive periods of drought stress by allowing a certain degree of cavitation.

Vergeynst et al. (2015*a*) excluded the initial decline in VWC versus water potential from their C calculations as it was attributed to water loss from open vessels at the cut branch ends and thus considered negligible. We, however, noted for *M. eminii* that this gentle slope was substantial and contributed to a C of $187 \pm 10 \, \text{kg m}^{-3} \, \text{MPa}^{-1}$ (Figure 3). Tyree and Yang (1990) postulated that capillary water, found in the lumens of inactive xylem elements and intracellular spaces, could be a possible source responsible for this initial drop in VWC and is usually released between -0.2 and $-0.5 \, \text{MPa}$ (Tyree and Ewers 1991). The initial decline in VWC for *M. eminii* took place between -0.9 and $-1.2 \, \text{MPa}$ (Figure 3) and with this increase in xylem tension, PLC increased from 0% to 2 % (Figure 1). The small change in PLC led us to presume that release of capillary water was the cause for this initial drop, which is considered to be a reversible process (Tyree and Ewers 1991). Furthermore, a high apparent modulus of elasticity (E_r') implies that a small decrease in water content is associated with a large decrease in cell water potential and turgor pressure (Kozlowski et al. 1991). *Maesopsis eminii* with an E_r' of 11 MPa that falls right in the middle of Bartlett et al. (2012)'s studied tropical species (between 5 and 30 MPa, except an outlier with an E_r' of $\sim 75 \, \text{MPa}$) has elastic cell walls that allows room for a greater water storage capacity (Sanchez-Diaz and Kramer 1971, Lambers et al. 1998) and

justifies the observed delay in declining water potential values (Figures 1 and 2) and its bendability.

Conclusively, this study highlights that for *M. eminii*, reliance on one sole commonly used parameter ψ_{50} to assess how vulnerable its xylem is to drought-induced cavitation may be misleading. This study therefore calls for the combined use of PLC, hydraulic capacitance, wood structural features and leaf strategies in the interpretation of a species' vulnerability to drought. It is also important to note that the findings of this study on branches cannot simply be extrapolated to mature trees and their wood, as a plant's structural and physiological properties change with age. However, the methodological framework and techniques presented in this article are transferrable regardless of age. More important also, this pioneering work on *M. eminii* has echoed the scarcity of studies within Africa's tropical terrestrial species, which seem to be endowed with novel unexplored traits that may ward off drought momentarily.

References

Anderegg WR (2015) Spatial and temporal variation in plant hydraulic traits and their relevance for climate change impacts on vegetation. New Phytol 205:1008–1014.

Asefi-Najafabady S, Saatchi S (2013) Response of African humid tropical forests to recent rainfall anomalies. Philos Trans R Soc B 368: 20120306.

Baranga D. (2007) Observations on resource use in Mabira forest reserve, Uganda. Afr J Ecol 45:2–6.

Barnard DM, Meinzer FC, Lachenbruch B, McCulloh KA, Johnson DM, Woodruff DR (2011) Climate-related trends in sapwood biophysical properties in two conifers: avoidance of hydraulic dysfunction through coordinated adjustments in xylem efficiency, safety and capacitance. Plant Cell Environ 34:643–654.

Bartlett MK, Scoffoni C, Sack L (2012) The determinants of leaf turgor loss point and prediction of drought tolerance of species and biomes: a global meta-analysis. Ecol Lett 15:393–405.

Begg JE, Turner NC (1970) Water potential gradients in field tobacco. Plant Physiol 46:343–346.

Binggeli P, Hamilton AC (1993) Biological invasion by *Maesopsis eminii* in the East Usambara forests, Tanzania. Opera Bot 121:229–235.

Boffa JM, Kindt R, Katumba B, Jourget JG, Turyomurugyendo L (2008) Management of tree diversity in agricultural landscapes around Mabira Forest Reserve, Uganda. Afr J Ecol 46:24–32.

Borchert R (1994) Soil and stem water storage determine phenology and distribution of tropical dry forest trees. Ecology 75:1437–1449.

Bouche PS, Larter M, Domec JC, Burlett R, Gasson P, Jansen S, Delzon S (2014) A broad survey of hydraulic and mechanical safety in the xylem of conifers. J Exp Bot 65:4419–4431.

Buchholz T, Tennigkeit T, Weinreich A (2010) Single tree management models: *Maesopsis eminii*. In: Bongers F, Tennigkeit T (eds) Degraded forests in Eastern Africa: management and restoration. Earthscan, London, UK and Washington, DC, USA, pp 247–266.

CABI (2016) *Maesopsis eminii* (umbrella tree). http://www.cabi.org/isc/?compid=5&dsid=32199&loadmodule=datasheet&page=481&site=144 (14 October 2016, date last accessed)

Carlquist S (1984) Vessel grouping in dicotyledon wood: significance and relationship to imperforate tracheary elements. Aliso 10: 505–525.

Chave J, Coomes D, Jansen S, Lewis SL, Swenson NG, Zanne AE (2009) Towards a worldwide wood economics spectrum. Ecol Lett 12: 351–366.

Choat B, Jansen S, Brodribb TJ et al. (2012) Global convergence in the vulnerability of forests to drought. Nature 491:752–755.

Christman MA, Sperry JS, Adler FR (2009) Testing the 'rare pit'hypothesis for xylem cavitation resistance in three species of acer. New Phytol 182:664–674.

Cochard H (1992) Vulnerability of several conifers to air embolism. Tree Physiol 11:73–83.

Cochard H, Badel E, Herbette S, Delzon S, Choat B, Jansen S (2013) Methods for measuring plant vulnerability to cavitation: a critical review. J Exp Bot 64:4779–4791.

De Roo L, Vergeynst LL, De Baerdemaeker NJF, Steppe K (2016) Acoustic emissions to measure drought-induced cavitation in plants. Appl Sci (Basel) 6:71. doi:10.3390/app6030071.

Domec JC, Gartner BL (2001) Cavitation and water storage capacity in bole xylem segments of mature and young douglas-fir trees. Trees 15: 204–214.

Edwards W, Jarvis P (1982) Relations between water content, potential and permeability in stems of conifers. Plant Cell Environ 5: 271–277.

Eggeling W (1947) Observations on the ecology of the budongo rain forest, uganda. J Ecol:20–87.

Gleason SM, Blackman CJ, Cook AM, Laws CA, Westoby M (2014) Whole-plant capacitance, embolism resistance and slow transpiration rates all contribute to longer desiccation times in woody angiosperms from arid and wet habitats. Tree Physiol 34:275–284.

Gleason SM, Westoby M, Jansen S et al. (2016) Weak tradeoff between xylem safety and xylem-specific hydraulic efficiency across the world's woody plant species. New Phytol 209:123–136.

Hacke UG, Sperry JS (2001) Functional and ecological xylem anatomy. Perspect Plant Ecol Evol System 4:97–115.

Hacke UG, Sperry JS, Pittermann J (2000) Drought experience and cavitation resistance in six shrubs from the great basin, utah. Basic Appl Ecol 1:31–41.

Hacke UG, Sperry JS, Pockman WT, Davis SD, McCulloh KA (2001) Trends in wood density and structure are linked to prevention of xylem implosion by negative pressure. Oecologia 126:457–461.

Hall JB (1995) Technical paper 13 *Maesopsis eminii* and its status in the East Usambara Mountains. Ministry of Tourism, Natural Resources and Environment, Dar es Salaam, Tanzania.

Hall JB (2010) Future options for *Maesopsis*: agroforestry asset or conservation catastrophe. In: Bongers F, Tennigkeit T (eds) Degraded forests in Eastern Africa: management and restoration. Earthscan, London, pp 221–245.

Hao GY, Hoffmann WA, Scholz FG, Bucci SJ, Meinzer FC, Franco AC, Cao KF, Goldstein G (2008) Stem and leaf hydraulics of congeneric tree species from adjacent tropical savanna and forest ecosystems. Oecologia 155:405–415.

Holbrook NM (1995) Stem water storage. In: Gartner BL (ed) Plant stems: physiology and functional morphology. Academic Press, San Diego, pp 151–174.

Hölttä T, Cochard H, Nikinmaa E, Mencuccini M (2009) Capacitive effect of cavitation in xylem conduits: results from a dynamic model. Plant Cell Environ 32:10–21.

Irvine J, Grace J (1997) Continuous measurements of water tensions in the xylem of trees based on the elastic properties of wood. Planta 202:455–461.

Jenkin RN, Howard WJ, Thomas P, Abell TMB, Deane GC (1977) Forestry development prospects in the Imatong Central Forest Reserve, southern Sudan Vol. 2 Main report. Land Resources Division, Tolworth.

Kozlowski TT, Kramer PJ, Pallardy SG (eds) (1991) The physiological ecology of woody plants. Academic Press, New York.

Lambers H, Chapin FS III, Pons TL (1998) Photosynthesis, respiration, and long-distance transport. In: Lambers H, Chapin FS III, Pons TL (eds) Plant physiological ecology. Springer, New York, USA, pp 10–153.

Loepfe L, Martinez-Vilalta J, Pinol J, Mencuccini M (2007) The relevance of xylem network structure for plant hydraulic efficiency and safety. J Theor Biol 247:788–803.

Markesteijn L, Poorter L, Paz H, Sack L, Bongers F (2011) Ecological differentiation in xylem cavitation resistance is associated with stem and leaf structural traits. Plant Cell Environ 34:137–148.

McCulloh KA, Johnson DM, Meinzer FC, Voelker SL, Lachenbruch B, Domec JC (2012) Hydraulic architecture of two species differing in wood density: Opposing strategies in co-occurring tropical pioneer trees. Plant Cell Environ 35:116–125.

Meinzer F, James S, Goldstein G, Woodruff D (2003) Whole-tree water transport scales with sapwood capacitance in tropical forest canopy trees. Plant Cell Environ 26:1147–1155.

Meinzer FC, Johnson DM, Lachenbruch B, McCulloh KA, Woodruff DR (2009) Xylem hydraulic safety margins in woody plants: coordination of stomatal control of xylem tension with hydraulic capacitance. Funct Ecol 23:922–930.

Muggeo VM (2008) Segmented: an r package to fit regression models with broken-line relationships. R News 8:20–25.

Niklas KJ (ed) (1992) Plant biomechanics: an engineering approach to plant form and function. University of Chicago Press, Chicago, USA.

Orwa C, Muta A, Kindt R, Jamnads R, Anthony S (2009) A tree reference and selection guide version 4.0. http://www.worldagroforestry.org/treedb/AFTPDFS/Maesopsis_eminii.PDF (14 October 2016, date last accessed).

Pammenter N, Van der Willigen C (1998) A mathematical and statistical analysis of the curves illustrating vulnerability of xylem to cavitation. Tree Physiol 18:589–593.

Pearson T, Burslem D, Goeriz R, Dalling J (2003) Regeneration niche partitioning in neotropical pioneers: effects of gap size, seasonal drought and herbivory on growth and survival. Oecologia 137:456–465.

Pineda-García F, Paz H, Meinzer FC (2013) Drought resistance in early and late secondary successional species from a tropical dry forest: the interplay between xylem resistance to embolism, sapwood water storage and leaf shedding. Plant Cell Environ 36:405–418.

Pittermann J, Sperry JS, Wheeler JK, Hacke UG, Sikkema EH (2006) Mechanical reinforcement of tracheids compromises the hydraulic efficiency of conifer xylem. Plant Cell Environ 29:1618–1628.

Rosner S, Karlsson B, Konnerth J, Hansmann C (2009) Shrinkage processes in standard-size norway spruce wood specimens with different vulnerability to cavitation. Tree Physiol 29: 1419–1431.

Rosner S, Světlík J, Andreassen K, Børja I, Dalsgaard L, Evans R, Karlsson B, Tollefsrud M, Solberg S (2013) Wood density as a screening trait for drought sensitivity in norway spruce 1. Can J Forest Res 44: 154–161.

Sanchez-Diaz MF, Kramer PJ (1971) Behavior of corn and sorghum under water stress and during recovery. Plant Physiol 48: 613–616.

Schabel HG, Latiff A (1997) *Maesopsis eminii* Engler. In: Faridah Hanum I, van Der Maesen LJG (eds) Plant resources of South-East Asia No. 11: Auxiliary plants. Backhuys, Leiden, The Netherlands, pp 184–187.

Schenk HJ, Steppe K, Jansen S (2015) Nanobubbles: A new paradigm for air-seeding in xylem. Trends Plant Sci 20:199–205.

Scholz A, Klepsch M, Karimi Z, Jansen S (2013) How to quantify conduits in wood. Front Plant Sci 4:1–11.

Shen F, Gao R, Liu W, Zhang W (2002) Physical analysis of the process of cavitation in xylem sap. Tree Physiol 22:655–659.

Sperry JS, Meinzer FC, McCulloh KA (2008) Safety and efficiency conflicts in hydraulic architecture: scaling from tissues to trees. Plant Cell Environ 31:632–645.

Steppe K, Lemeur R (2007) Effects of ring-porous and diffuse-porous stem wood anatomy on the hydraulic parameters used in a water flow and storage model. Tree Physiol 27:43–52.

Steppe K, Cochard H, Lacointe A, Ameglio T (2012) Could rapid diameter changes be facilitated by a variable hydraulic conductance? Plant Cell Environ 35:150–157.

Tyree MT, Ewers FW (1991) The hydraulic architecture of trees and other woody plants. New Phytol 119:345–360.

Tyree MT, Yang S (1990) Water-storage capacity of thuja, tsuga andacer stems measured by dehydration isotherms. Planta 182:420–426.

Vergeynst LL, Dierick M, Bogaerts JA, Cnudde V, Steppe K (2015*a*) Cavitation: a blessing in disguise? New method to establish vulnerability curves and assess hydraulic capacitance of woody tissues. Tree Physiol 35:400–409.

Vergeynst LL, Sause MG, Hamstad MA, Steppe K (2015*b*) Deciphering acoustic emission signals in drought stressed branches: the missing link between source and sensor. Front Plant Sci 6. doi:10.3389/fpls.2015.00494.

Vergeynst LL, Sause MG, De Baerdemaeker NJ, De Roo L, Steppe K (2016) Clustering reveals cavitation-related acoustic emission signals from dehydrating branches. Tree Physiol. 36:786–796.

Wheeler JK, Huggett BA, Tofte AN, Rockwell FE, Holbrook NM (2013) Cutting xylem under tension or supersaturated with gas can generate plc and the appearance of rapid recovery from embolism. Plant Cell Environ 36:1938–1949.

Worbes M, Staschel R, Roloff A, Junk W (2003) Tree ring analysis reveals age structure, dynamics and wood production of a natural forest stand in cameroon. For Ecol Manage 173:105–123.

Zimmermann M (1983) Xylem structure and the ascent of sap. Springer, Berlin.